ISSN: 2278-4632
Vol-13, Issue-07, July 2023

A Novel Fuzzy Logic Controller of Winding Based DC-Bus Capacitor Discharge for PMSM Drives in Electric Vehicles

P. DEELAJA KUMARI[1] & S. SRIDHAR[2]

[1]PG Scholar, [2]Assistant Professor
Dept. of Electrical and Electronics Engineering (Power & Industrial Drives),
Jawaharlal Nehru Technological University College of Engineering Anantapur, India
Mail Id: pdeelajakumari@gmail.com[1], sridharsavarapu.eee@jntua.ac.in[2]

ABSTRACT

This paper presents the implementation of Fuzzy Logic Controller winding based DC Bus Capacitor Discharge for PMSM Drives in the Electric Vehicle applications. For the purpose of reducing the bus voltage to safe voltage as soon as possible,the discharge method can be divided into two phases, rapid discharge stage and bus voltage regulation stage. Firstly, the dc-bus voltage will be dropped to safe voltage due to the large flux-weakening current applied to the d-axis. Secondly, in order to stabilize the bus voltage at safe voltage, an extended observer state (ESO) is designed to estimate and compensate the total power loss that is regarded as disturbance in busvoltage regulation stage. The parameters of the proposed ESO are designed and the tracking performance isanalysed. The simulation results are evaluated by using MATLAB/SIMULINK software.

INDEX TERMS: Permanent magnet synchronous machine (PMSM), winding-based discharge, dc-bus discharge, extended state observer, Fuzzy Logic Controller (FLC).

I. INTRODUCTION

Recently, the electric vehicles (EVs) are becoming more andmore prevalent in our life on account of energy-saving and zero pollution-emission operation [1]–[4]. Permanent magnet synchronous motor (PMSM) has been widely used as the powertrain in the electric vehicle for the advantages of high efficiency, high power density and high torque to current ratios [5]–[9]. Furthermore, in order to improve the PMSM driving efficiency and reduce the PMSM driving currents, high voltage driven systems are extensively adopted in electric vehicles [10]. However, high voltage powertrains wouldexpose driver to electric shock risks when EVs happens to an emergency such as car crash. In response to this problem,United Nation Vehicle Regulation ECC R94 requires that the dc-bus capacitor voltage should drop to safe voltage (60V) less than 5 seconds [11]. When the EVs encounter an accident, the breaker will be triggered and the motor is disengaged from the clutch, leading the motor operates freely. Although the drive system has been disconnected from the battery at this time, the back electro- motive force (EMF) of PMSM and the remaining energy of the bus capacitor will maintain the dc-bus voltage at a high voltage for a long time.

Hence, the EVs drive system usually add a discharge circuit that used to active discharge the dc-bus capacitor as soon as possible. Generally, the discharge circuit consist ofa power switch and a bleeding resister, which is paralleledto the dc-bus The schematic diagram of the commonly usedEVs power actuating system is shown in Fig.1.
Although the small bleeding resister can make the dis- charge time meet the United Nation Vehicle Regulation ECC R94 requirements that less than 5s, it will lead bleeding resister volume is large and fragile [12]. More importantly, when an emergency happens to electric vehicles, the bleeding resister may be broken or faulted, which exposing passengers and rescuers at risk of electric shocks. As for the EVs safety a doable solution to this situation is to incorporate discharge circuit fault handling

ISSN: 2278-4632
Vol-13, Issue-07, July 2023

techniques, which can make discharge process meet the requirements that five-second discharge and no voltage surge.

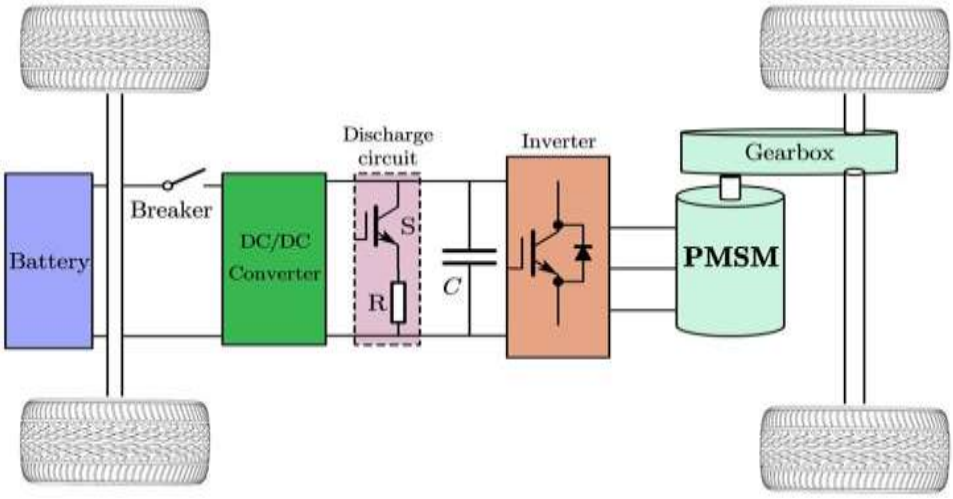

Figure 1. Topology of EVs-PMSM powertrain system.

Due to the bleeder resister cannot work for dissipatingthe residual energy in the capacitor, the motor windings or the inverter can be used to discharge the dc-bus capacitor.In [13], the dc-bus capacitor energy is dissipated in the form of heat by shorting the inverter, which turn on the MOSFETsor IGBTs of one or more bridge in the inverter at the same time to constitute a short circuit. Although this method can prevent the kinetic energy of motor flowing into the capacitor,it will lead to large discharge current which may damagethe inverter. Hence this method has been rarely used in practice. The winding-based discharge method can not only reduce the volume of the discharge circuit but also be cost- effective [14]–[16]. In [14], the dc-bus capacitor voltage is discharged by injecting a constant large *d* -axis current and a zero *q*-axis current. However, this method can be only used in the low-speed region that the EMF is lower than the safe volt-age, otherwise the dc-bus capacitor will be recharged, which pose a great risk to the PMSM driving system and the passengers. For the sake of avoiding the voltage surge phenomenonand discharging the dc-bus voltage as soon as possible,[15] propose a three stages discharge method based on voltage regulation regardless of the electric machine speed. In order to prevent the bus voltage being recharged, a dc-busvoltage regulator based on a proportional integral controllertogether with a modulation index controller is adopted to generate the reference *d* -axis current. Aiming at discharging the capacitor voltage of particular EVs driven system with large inertia and small safe current, a fixed d-axis current and piecewise q-axis current control is proposed in [16].

Although the method in [15] and [16] have been utilizedto some occasions, models in the algorithm is imprecise and parametric robustness is not considered. More importantly, the resistance and inductance of the machine are very sensitive to temperature, which makes their values change drastically during the discharge process when using the windings as the bleeder. This side effect can lead to prolonged dis-charge time or voltage surges. Additionally, the three-phasePWM rectifier model is nonlinear in synchronous reference frame, which lead the PI-based strategy cannot be applied tothe system.

This study aims to propose a robust dc-bus capacitor discharge technique for the EVs PMSM drives under the discharge circuit fault. The proposed robust active dischargemethod is divided into two stages when the EVs happens emergency. At the first stage, a large *d* -axis current and zero *q*-axis current are employed to rapidly reduce the bus voltageto safe voltage by reducing the back EMF of the PMSM. When the dc-bus voltage reaches 60V, the second stage starts, and the control strategy switch from direct current controlto voltage control, thus the voltage is stabilized by applying ESO

ISSN: 2278-4632
Vol-13, Issue-07, July 2023

to observe the dc-bus capacitor energy until the voltagereduce to 0. ESO is a part of active disturbance rejection observer, which is firstly proposed by Han [17]. The main idea of the ESO is regarding the inner and outer non-linearity, uncertain part of the model and disturbance of the system as total disturbance. The total disturbance is treated as a new variable, which can be estimated and compensatedby feed forward.

Considering that as the speed decreases, the backEMF will also decrease, hence a speed dependent ESO is designed to observe the total loss of system and parameter vibration which is regarded as total disturbance in the secondstage. The observed total disturbance is compensated to the dc-bus capacitor energy loop control law in real time in orderto realize the dc-bus voltage constant and avoid the voltage surges.

This article is organized as six sections. In Section II,the mathematical model of the winding-based discharge is presented. Section III describes the proposed robust winding-based discharge method. Section IV studies the ESO parameters design and performance. In Section V, the effectiveness of the method is verified by simulation. Finally, the conclusion is given in Section VI.

II. MATHEMATICAL MODEL OF THE WINDING-BASED DISCHARGE METHOD

This section mainly analyzes the winding-based method and constructs the discharge model. If an emergency occurs to the EVs, the energy should be dissipated not only the energystored in the dc-bus capacitor but also the kinetic energyof Without considering non-linearity and hysteresis effect of iron corn in the SPMSM/G, a simple model can be derived and transformed to the synchronous reference frameas [18]–[20]:

$$\left.\begin{aligned} u_d &= R_s i_d + L_s \frac{di_d}{dt} - \omega_e L_s i_q \\ u_d &= R_s i_d + L_s \frac{di_q}{dt} - \omega_e L_s i_d + \omega_e \psi_f \\ T_e &= \frac{3}{2} p \psi_f i_q \end{aligned}\right\} \quad (1)$$

Where $i_{d,q}$ and $u_{d,q}$ are d -, q-axis stator currents and voltages, respectively. R_s is the stator resistance, and L_s the stator inductance. ω_e is electrical angular velocity. p is the pole pair number. ψ_f is the flux linkage of the PMSM/G. T_e is the electromagnetic torque.

The mechanical equation of the permanent magnet synchronous motor can be expressed as

$$J \frac{d\omega_m}{dt} = T_e - B_m \omega_m \quad (2)$$

where ω_m is the mechanical angular velocity, J and B_m are inertia and mechanical damping coefficient respectively.

According to the reference direction relation of capacitor current shown in Fig. 2, the dynamic equation of capacitor voltage u_{dc} can be expressed as

$$C \frac{du_{dc}}{dt} = i_{dc} \quad (3)$$

ISSN: 2278-4632
Vol-13, Issue-07, July 2023

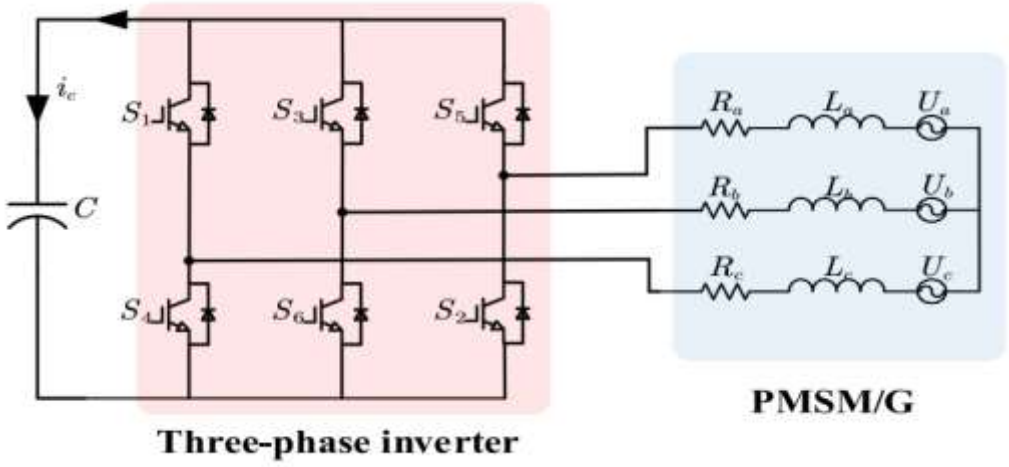

Figure 2: Schematic diagram of winding-based dc-bus capacitor discharge.

where C is the capacitor, i_{dc} and u_{dc} are the dc-bus current and voltage, respectively. Considering the power loss of the converter, the power of the AC side should equal to the power of the DC side, that is

$$u_{dc}i_{dc} + P_{con} = -\frac{3}{2}\left(u_d i_d + u_q i_q\right) \tag{4}$$

where P_{con} is the switching loss of the IGBT devices.

In order to analyze the power flow process during dis- charge, substitute (1) and (3) into the instantaneous power balance (4). Then, (5) is derived

$$\frac{d}{dt}\left(\frac{1}{2}Cu_{dc}^2\right) = -\frac{3}{2}\omega_e\psi_f i_q - \frac{3}{2}R_s\left(i_d^2 + i_q^2\right) - \frac{3}{2}\left(L_s i_q\frac{di_q}{dt} + L_s i_d\frac{di_d}{dt}\right) - P_{con} \tag{5}$$

The above formula shows that part of the electromagnetic power output of the permanent magnet synchronous motor is transformed to inductance coil energy, copper loss of wind- ings and the converter loss. Then the residual is used to adjust the capacitor energy storage.

III. THE PROPOSED ROBUST WINDING BASED DISCHARGE METHOD

For the purpose of achieving a reliable and safe discharge method when the EVs encounter an emergency with active discharge circuit fault, it is important to redesign a robust discharge approach. Thereby, a robust winding-based dc-bus capacitor discharge method based on ESO is presented in this part.

A. RAPID DISCHARGE STAGE

It is meaningful and safe to the passengers and rescuers if the dc-bus voltage can drop to safe levels immediately when an active discharge is requested. As the motor speed is higher when the electric vehicles encounter an emergency, the back electromotive force (EMF) is larger than safe voltage. Due to the dc-bus capacitor voltage track the back EMF, the dc-bus capacitor voltage can drop to safe voltage when the back EMF is reduced to safe voltage. As the dc-bus voltage is approximately proportional to the EMF of the PMSM, a large d-axis current is injected to quickly reduce the EMF based on flux-weakening principle, and the q-axis current keep at zero at the moment in order to prevent the kinetic energy being converted into electrical energy [21]. In order to reduce the analytical complexity, according to [22], the bus voltage can be expressed as

ISSN: 2278-4632
Vol-13, Issue-07, July 2023

$$u_{dc} = \sqrt{3}\omega_e(\psi_f + L_s i_d) - R_s\sqrt{i_d^2 + i_q^2} - 2V_{on} \quad (6)$$

where V_{on} is the diode conducted voltage. In the first stage, the voltage should drop to safe voltage. Hence, the d-axis flux-weakening current is

$$i_d^* = \frac{U_{safe} - \sqrt{3}\omega_e\psi_f}{(\sqrt{3}\omega_e L_s + R_s)} \quad (7)$$

where U_{safe} is safe voltage.

Therefore, the dc-bus voltage can be dropped to the safe voltage with the calculated d-axis current injected once the active discharge is required. Simultaneously, a zero q-axis current is applied in order to prevent any electromagnetic power converting into electrical energy. A PI controller is applied to confirm that the machine current can track the calculated d-, q- axis current in real time.

B. BUS VOLTAGE CONTROL STAGE BASED ON ESO

When the dc-bus voltage reaches 60V, the ESO-based voltage control stage starts. In order to maintain the voltage at safe voltage, a voltage loop based on robust control is designed.
Obviously, the energy flow process in discharge mode of (5) is nonlinear, which the PI controller cannot achieve satisfactory results, especially the motor parameters will change in the process of discharging. Here, we will introduce an ESO-based ultra local model to resolve the problem.

For the purpose of converting the equation (5) to an integral series system, the first-order ultra control model of a single-input and single-out system can be expressed as [23]–[25]

$$\dot{y} = F + \alpha u \quad (8)$$

where u is control variables, y is the output variables, α is a nonphysical scaling factor selected by the designer and the F represents the known and unknown part of the system. In this article, according to formulas (5) and (8), hence the mathematical model of the energy flow based ESO can be expressed as

$$\frac{dE_c}{dt} = F + \alpha u \quad (9)$$

where $E_c = 0.5Cu_{dc}^2$ u = i_q, $\alpha = -1.5\omega_e\psi_f$ and the other of terms on the right side of (5) except $-1.5\omega_e\psi_f i_q$ are treated as the total disturbance and notated as F

$$F = -\frac{3}{2}R_s(i_d^2 + i_q^2) - \frac{3}{2}\left(L_s i_q \frac{di_q}{dt} + L_s i_d \frac{di_d}{dt}\right) - P_{con} \quad (10)$$

Equation (10) indicts the total disturbance present total power loss, which consist of switching loss, windings copper loss and inductance coil energy storage. And assume that F is constant during every sampling period.

A linear ESO that taking E_c and F as variables can be constructed as (11) based on the ultra-local model of (8).

$$\left.\begin{aligned} e_1 &= z_1 - E_c \\ \dot{z}_1 &= z_2 - \beta_1 e_1 + \alpha u \\ \dot{z}_2 &= -\beta_2 e_2 \end{aligned}\right\} \quad (11)$$

where z_1 and z_2 are the estimated value of E_c and F respectively. β_1 and β_2 are feedback gains respectively. Therefore, the block diagram of ESO is shown in Fig. 3.

ISSN: 2278-4632
Vol-13, Issue-07, July 2023

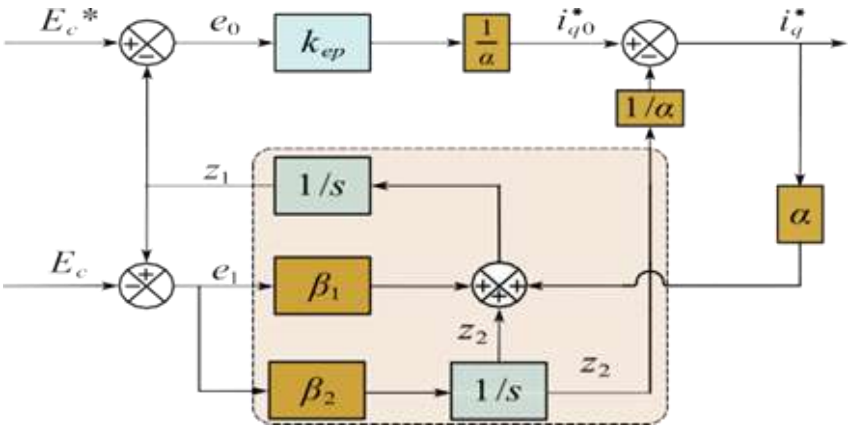

Figure 3. Block diagram of ESO

According to [17], if the gains β_1 and β_2 are properly chosen, the formula (11) can estimate the real-time valuesof E_c and F that is, $z_1 \rightarrow E_c, z_2 \rightarrow F$.

C.POWER LOOP CONTROL LAW DESIGN

In order to maintain the dc-bus voltage at safe voltage,the estimated total power loss should be compensated beforethe input of the plant.

Therefore, the control law can be expressed as follows:

$$i_q^* = \frac{i_{q0}^* - z_2}{\alpha} \tag{12}$$

where i_{q0} is the initial plant input based on the initial control law. Substituting (12) into (9) yields

$$\frac{dE_c}{dt} = \alpha i_{q0}^* + F - z_2 \tag{13}$$

When the estimated value z_2 approaches F

$$\frac{dE_c}{dt} = \alpha i_{q0}^* \tag{14}$$

Consequently, a proportional power controller is designed as (15), converting the energy error into power loss, which is compensated by estimated total power loss of ESO.

$$i_{q0}^* = \frac{k_{ep}\left(E_c^* - \hat{E}_c\right)}{\alpha} \tag{15}$$

where k_{ep} is the gain of power loop. Hence the power loop control law based on ESO can be expressed as follows

$$\left.\begin{aligned} e_0 &= E_c^* - z_1 \\ i_{q0}^* &= \frac{k_{ep} e_0}{\alpha} \\ i_q^* &= i_{q0}^* - \frac{z_2}{\alpha} \end{aligned}\right\} \tag{16}$$

where E_c^* is the reference value of E_c.

With the dc-bus voltage controller based on ESO, the overall block diagram of the proposed robust dc-bus capacitor discharge strategy is presented in Fig.4 demonstrate the schematic diagram of the traditional and proposed discharge method. Two virtual switches are applied to select operation of the system. The port 1 is connected when the system work in driving mode. At this time, the control method of the PMSM can be vector control or direct torque control.

Once the drive system receives the active discharge requirement, the port 2 is connected and the robust winding-based discharge method is implemented. In order to make real-time current can quickly track the given current when the system work in normal operation and discharge mode, two

ISSN: 2278-4632
Vol-13, Issue-07, July 2023

PI controllers are used in d-, q- axis current loop and the parameter is designed according to [26] in this article.

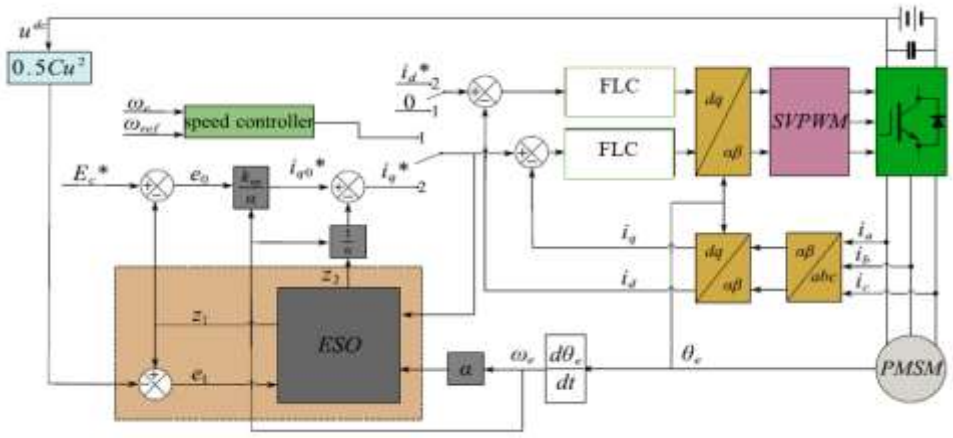

Figure 4: Overall block diagram of the FLC of winding-based dc-bus capacitor discharge strategy.

The total discharge process is shown in Fig.5. The dc-bus capacitor voltage drops to safe voltage when the large d-axis current is injected at t_1. Once the voltage reaches at safe voltage at t1, the voltage regulation stage is started, which the dc-bus voltage has been stable at safe voltage until t_2. Starting from t_2, the back EMF is smaller than the safe voltage because of the speed drop to low speed.

IV. ESO PARAMETERS DESIGN AND PERFORMANCE ANALYSIS

The performance of the proposed strategy is discussed in this part. First of all, the stability and parameters design of the ESO is investigated. Secondly, the tracking performance of the proposed ESO-based strategy are concluded. In the proposed strategy, the gain of β_1 and β_2 is very crucial for the system performance, so the parameters are investigated firstly.

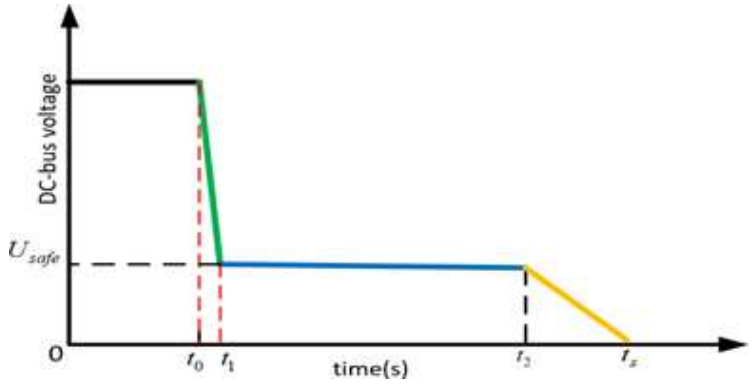

Figure 5. Discharge process of proposed discharge method.

A. PARAMETERS DESIGN FOR ESO

Equation (11) can be rewritten in matrix form as

$$\left.\begin{aligned}\dot{z} &= Az + Bu + D(y - \hat{y})\\ \hat{y} &= Cz\end{aligned}\right\} \tag{17}$$

ISSN: 2278-4632
Vol-13, Issue-07, July 2023

where $z = [z_1 \quad z_2]^T$, $A = \begin{bmatrix} 0 & 1 \\ 0 & 0 \end{bmatrix}$, $B = \begin{bmatrix} \alpha \\ 0 \end{bmatrix}$, $C = [1 \quad 0]$, $D = [\beta_1 \quad \beta_2]^T$

Let e = $[z_1 - E_c, z_2 - F]^T$ be the tacking error of the ESO. According to (9) and (17), the error state equation can be derived as

$$\dot{e} = A_m e \tag{18}$$

where $A_m = \begin{bmatrix} -\beta_1 & 1 \\ -\beta_2 & 0 \end{bmatrix}$. Equation (18) shows that characteristic equation of the ESO is determined by the eigenvalues of A_m. Hence, when $\beta_2 > 0$, the error dynamics (18) is asymptotically stable. The parameters of ESO can be designed according to the desired bandwidth. More importantly, the following equation should be satisfied

$$|sI - A_m| = s^2 + \beta_1 s + \beta_2 = (s + \omega_0)^2 \tag{19}$$

where I represent the identity matrix. Hence

$$\left.\begin{aligned} \beta_1 &= 2\omega_0 \\ \beta_2 &= \omega_0^2 \end{aligned}\right\} \tag{20}$$

where ω0 is the bandwidth of the ESO. And the bandwidth determines the performance of the observer tracking the total disturbance Therefore, ESO parameters can be determined once the bandwidth has been confirmed.

B. TRACKING PERFORMANCE ANALYSIS FOR ESO

Estimation and compensation of the system disturbance is important to improve the robustness. According to (11), the error between the original system and the ESO is derived as

$$\left.\begin{aligned} e_1 = z_1 - E_c, e_2 &= z_2 - F \\ \dot{e}_1 &= e_2 - \beta_1 e_1 \\ \dot{e}_2 &= -\beta_2 e_1 - \dot{F} \end{aligned}\right\} \tag{21}$$

It transformed to s-domain and express as

$$\left.\begin{aligned} s e_1(s) &= e_2(s) - \beta_1 e_1(s) \\ s e_2(s) &= -\beta_2 e_1(s) - \dot{F}(s) \end{aligned}\right\} \tag{22}$$

According equation (22), the following transfer function can be obtained as

$$\frac{z_1(s)}{E_c(s)} = \frac{2\omega_0 s + \omega_0^2}{s^2 + 2\omega_0 s + \omega_0^2} \tag{23}$$

$$\frac{z_2(s)}{E_c(s)} = \frac{\omega_0^2}{s^2 + 2\omega_0 s + \omega_0^2} \tag{24}$$

Then the transfer function between the output error and the estimated total disturbance is

$$\frac{e_1(s)}{F(s)} = \frac{s}{s^2 + 2\omega_0 s + \omega_0^2} \tag{25}$$

Therefore, the transfer function between the estimated total disturbance error and the estimated total disturbance is

$$\frac{e_2(s)}{F(s)} = \frac{s^2 + 2\omega_0 s}{s^2 + 2\omega_0 s + \omega_0^2} \tag{26}$$

In order to analyse the effect of bandwidth for the estimation accuracy and select the proper value, the bode diagrams of the corresponding transfer function are presented in Fig.6 Fig. 6 (a) and (b) show that the bandwidth of the ESO has significant impact on total disturbance and capacitor energy estimation accuracy. Fig. 6 (c) and (d) indicate that the bandwidth is higher, the disturbance estimation

ISSN: 2278-4632
Vol-13, Issue-07, July 2023

error smaller. By properly tuning the parameters of β1 and β2, the ESO can achieve fast tracking performance and estimation error smaller. The diagrams also show that Fig. 6 (c) and Fig. 6 (d) has very low gain while the ESO has a good estimation accuracy, which prove that the ESO has strong robustness and disturbance rejection capabilities. Therefore, the inner dynamic analysis the ESO can track variables and total system disturbances accurately and quickly. Although a large ω0 show better low frequency suppression effect, but too large ω0 will introduce extra noise in a practical system. Thus, there exist a compromise for the selection of ω0.

closed-loop transfer function is derived with considering current inner loop and ESO. As the inner current loop can be expressed as (27) in the frequency domain of q-axis.

$$u_q^* = \left(k_{cp} + \frac{k_{ci}}{s}\right)\left(i_q^*(s) - i_q(s)\right) + \omega_e L_d i_d(s) + \omega_e \psi_f \tag{27}$$

According to feedback control law, the inner loop given can be expressed as

$$\alpha i_q^*(s) = k_{ep}[E_c^*(s) - E_c(s)] - z_2(s) \tag{28}$$

Then, transforming (9) to s-domain and derived as

$$sE_c(s) = F(s) + \alpha i_q(s) \tag{29}$$

Substituting (27), (28) and (29) into the (1), which gives the following:

$$D(s)E_c(s) = N_1(s)E_c^*(s) + N_2(s)F(s) \tag{30}$$

where

$$\begin{cases} D(s) = a_0 s^5 + a_1 s^4 + a_2 s^3 + a_3 s^2 + a_4 s + a_5 \\ N_1(s) = b_0 s^3 + b_1 s^2 + b_2 s + b_3 \\ N_2(s) = c_0 s^4 + c_1 s^3 + c_2 s^2 + c_3 s \end{cases}$$

$$\begin{cases} a_0 = L_s, a_1 = \beta_1 L_s + k_{cp} + R_s \\ a_2 = k_{ci} + \beta_1 k_{cp} + \beta_1 R_s + \beta_2 L_s + k_{cp} k_{ep} \\ a_3 = \beta_2 k_{cp} + \beta_2 R_s + \beta_1 k_{ci} + \beta_1 k_{cp} k_{ep} + k_{ci} k_{ep} \\ a_4 = \beta_2 k_{ep} k_{cp} + \beta_2 k_{ci} + \beta_1 k_{ci} k_{ep}, a_5 = \beta_2 k_{ep} k_{ci} \\ b_0 = k_{cp}, b_1 = \beta_1 k_{cp} + k_{ci} \\ b_2 = \beta_2 k_{cp} + \beta_1 k_{ci}, b_3 = \beta_2 k_{ci} \\ c_0 = L_s, c_1 = \beta_1 L_s + k_{cp} + R_s \\ c_2 = k_{ci} + \beta_1 k_{cp} + \beta_1 R_s + \beta_2 L_s, \\ c_3 = \beta_1 k_{ci} + \beta_2 R_s \end{cases}$$

According to (30), the closed-loop system transfer function can be derived as:

$$G_1(s) = \frac{E_c(s)}{E_c^*(s)} = \frac{N_1(s)}{D(s)} \tag{31}$$

$$G_2(s) = \frac{E_c(s)}{F(s)} = \frac{N_2(s)}{D(s)} \tag{32}$$

G1(s) reflects the tracking performance of the controller and G2(s) reflects the anti-disturbance ability for the proposed method. More importantly, the numerator and denominator of the transfer function does not contain any terms related to speed, which demonstrate that the proposed method can stabilize dc-bus with speed decrease. Fig.7 and Fig.8 show that the dominant pole distribution diagram and the bode diagrams of $\frac{E_c(s)}{E_c^*(s)}$.

ISSN: 2278-4632
Vol-13, Issue-07, July 2023

The pole-zero map show that the closed-loop poles with the proposed method are all on the left half s-plane, which demonstrates the system is always stable. The arrows in Fig. 7 and Fig.8 represent the direction of k_{cp} increase. In addition, due to the bandwidth of ESO is selected as ω_0 there is a pair of zero and pole located at the ω_0. The closed-loop poles are moving as the gain range from 80 to 400. As can be seen from Fig. 7, the tracking performance is better with the larger gain obviously. However, when the gain value is larger than 320, the system will introduce two conjugate virtual roots, which will increase system oscillation. Fig. 9 indicts that the lager the k_{ep}, the better low frequency suppression effect. In order to enhance stability and tracking performance, with the dominant pole away from the imaginary axis, the value of k_{ep} is chosen to be 320. For the purpose of studying the sensitivity of transfer function from system total disturbance to output capacitor energy, the bode diagram is shown in Fig. 8. The bode diagram shows that the total disturbance effect can be suppressed by compensating the estimated z2 whether in high frequency or low frequency. And the bode diagram also proves that the designed ESO parameters is reasonable, the control method can keep stable and robust in a wide range.

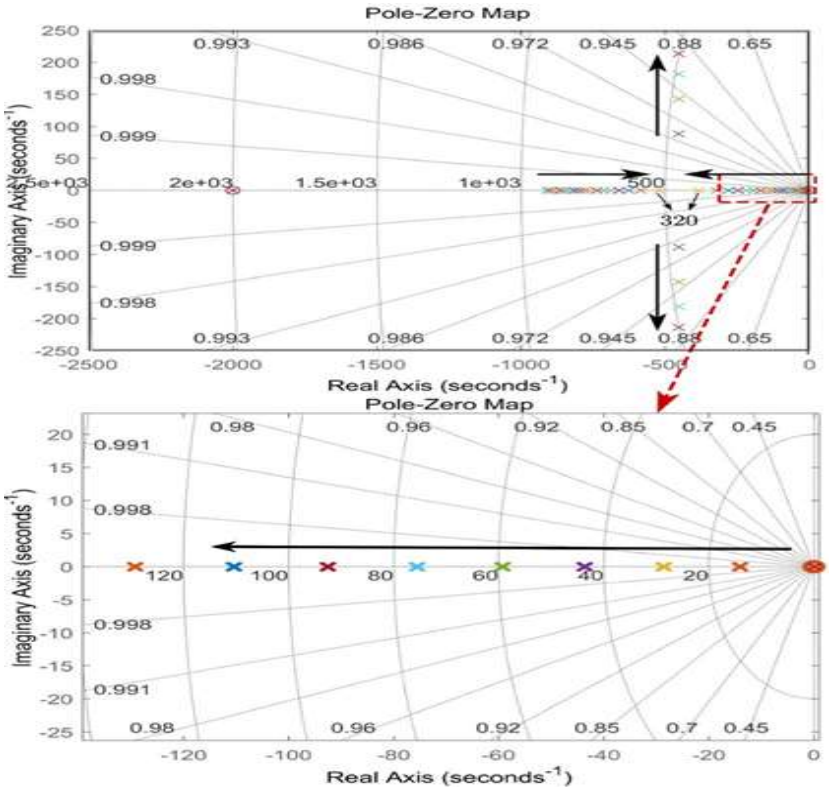

Figure 6: Pole-Zero Map of $G_1(s)$ ($0 < kep < 450$, $\omega_0 = 2000$)

ISSN: 2278-4632
Vol-13, Issue-07, July 2023

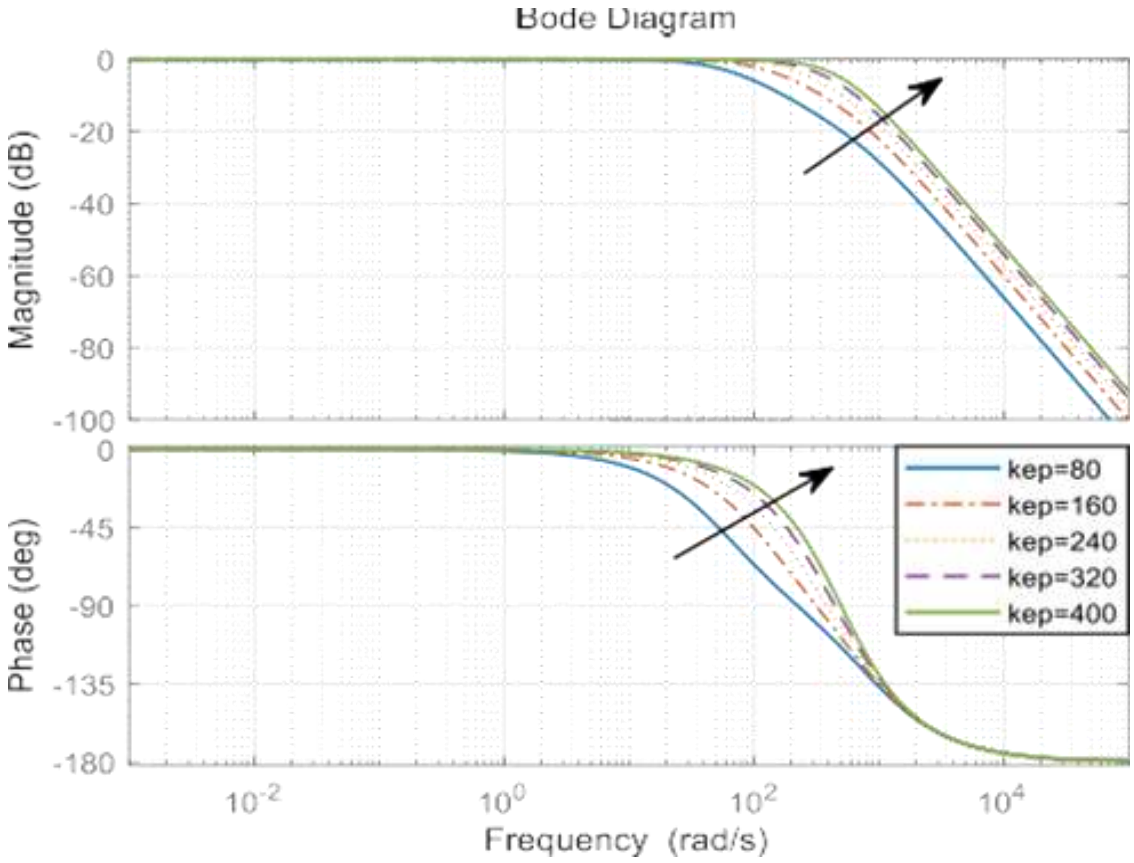

Figure 7: Bode diagram of $G_1(s)$ ($0 < kep < 450$, $\omega_0 = 2000$).

V. IMPLEMENTATION OF FUZZY LOGIC CONTROLLER

One of the reasons for the popularity of Fuzzy Logic Controllers is its logical resemblance to a human operator.

Components of FLC:

The inputs to a Fuzzy Logic Controller are the processed with the help of linguistic variables which in turn are defined with the aid of membership functions. The membership functions are chosen in such a manner that they cover the whole of the universe of discourse. To avoid any discontinuity with respect to minor changes in the inputs, the adjacent fuzzy sets must overlap each other. Because of a small time constant in Fuzzy Logic Controllers, this criterion is very important in the design of the same.
There are basically three essential segments in Fuzzy Logic Controller viz.

1. Fuzzifier.
2. Inference System.
3.Defuzzifier.

ISSN: 2278-4632
Vol-13, Issue-07, July 2023

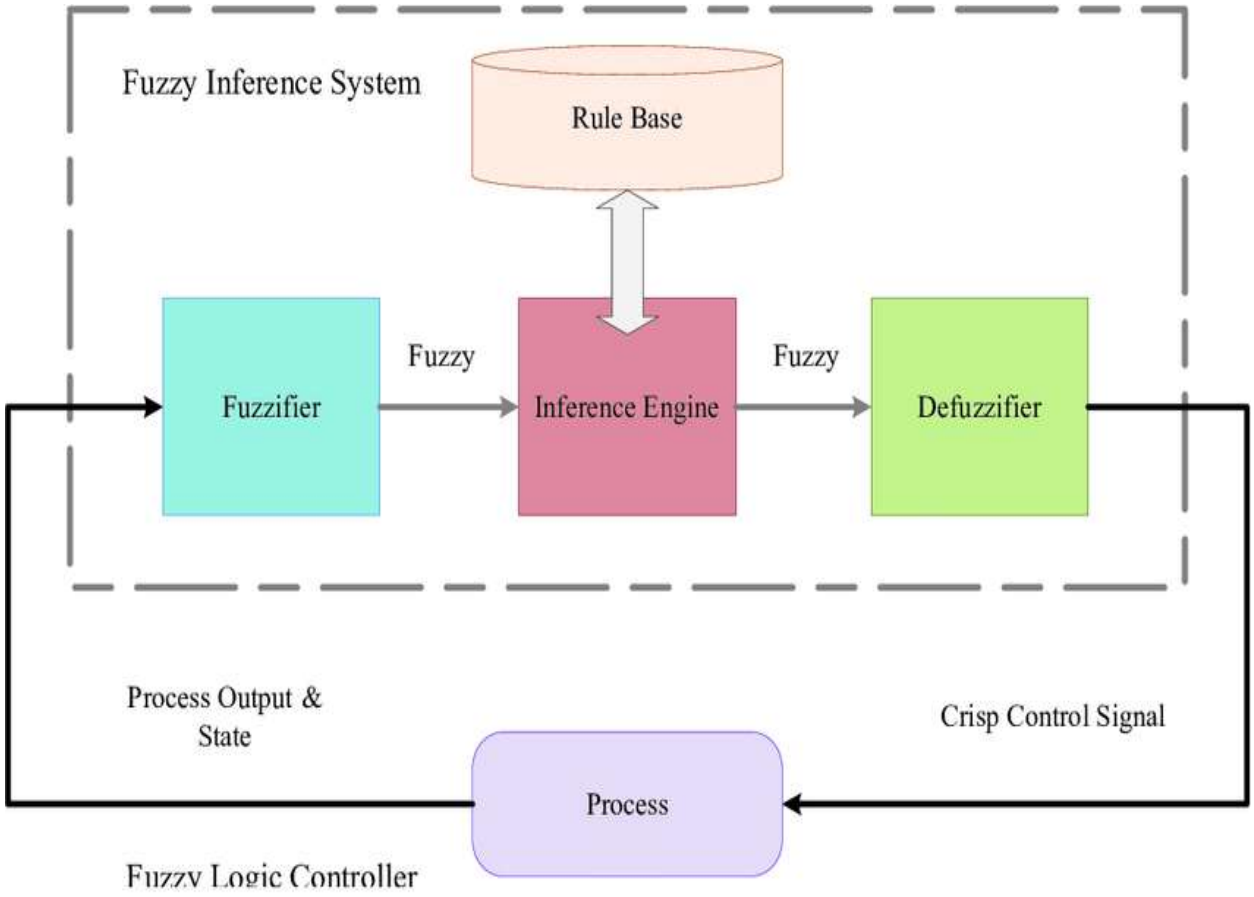

Figure 8: Fuzzy Logic Controller Structure

u	NB	NM	NS	ZO	PS	PM	PB
NB	PB	PB	PB	PB	PB	PB	PB
NM	PB	PB	PM	PM	PM	PB	PB
NS	PB	PM	PS	PS	PS	PM	PB
ZO	PB	PM	PS	ZO	PS	PM	PB
PS	PB	PM	PS	PS	PS	PM	PB
PM	PB	PB	PM	PM	PM	PB	PB
PB	PB	PB	PB	PB	PB	PB	PB

ISSN: 2278-4632
Vol-13, Issue-07, July 2023

V.SIMULATION RESULTS

SIMULATION BLOCK DIAGRAM:

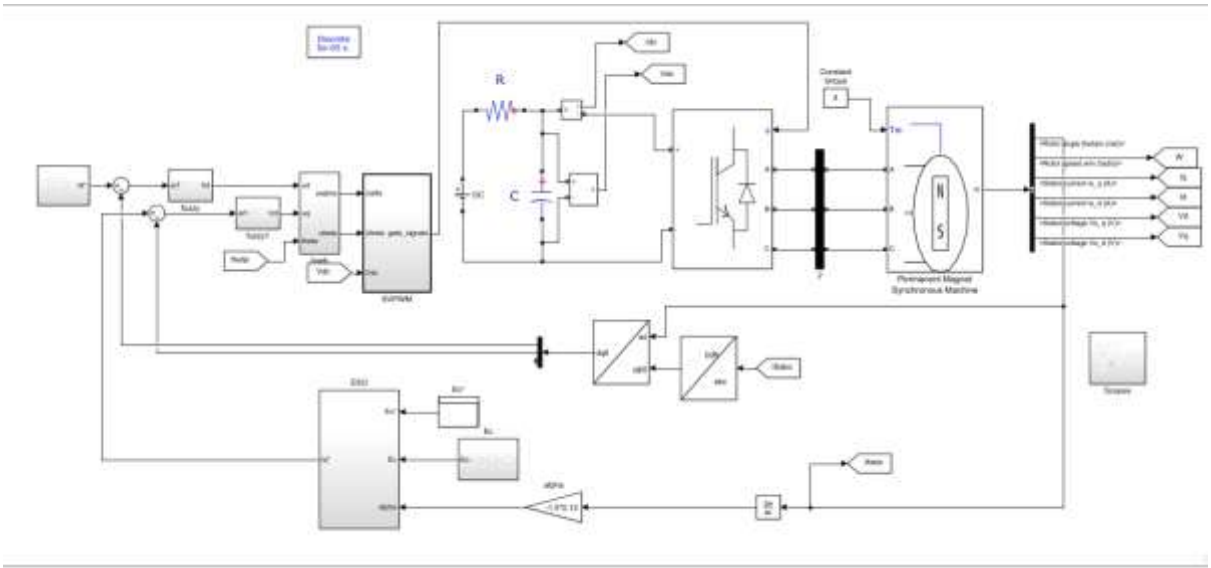

Figure 9: Proposed Simulink

In order to validate the proposed discharge algorithm, the simulation and experiment were conducted and the results presented in this section.

SIMULATION RESULTS:

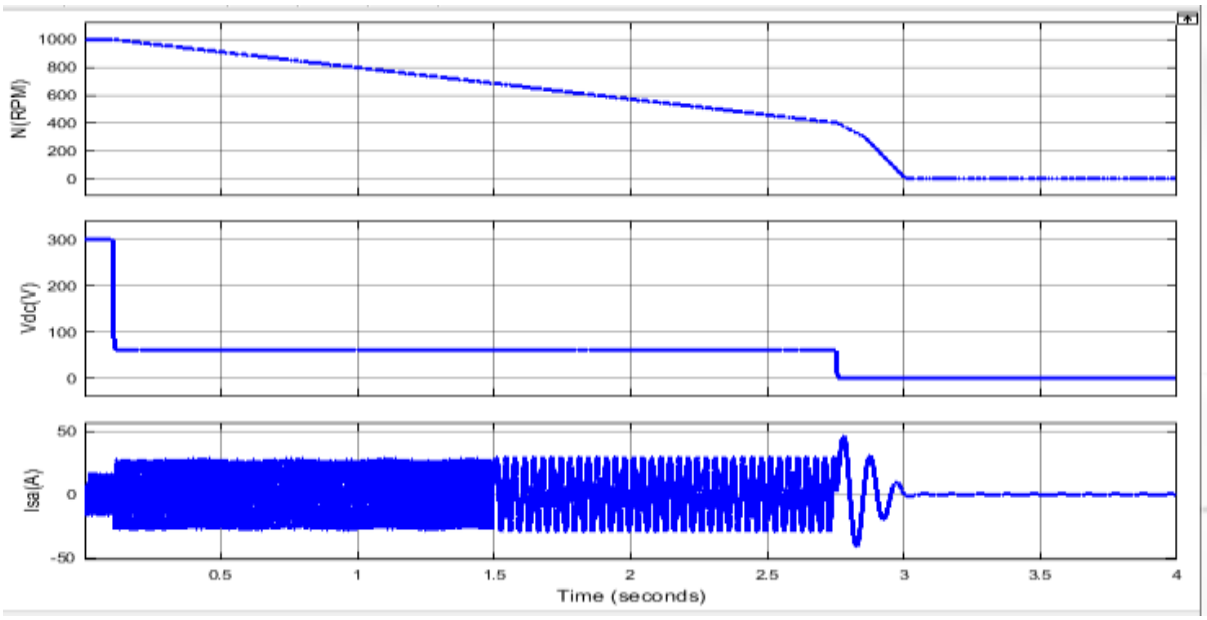

Figure 10: Waveforms of dc-bus capacitor discharge

ISSN: 2278-4632
Vol-13, Issue-07, July 2023

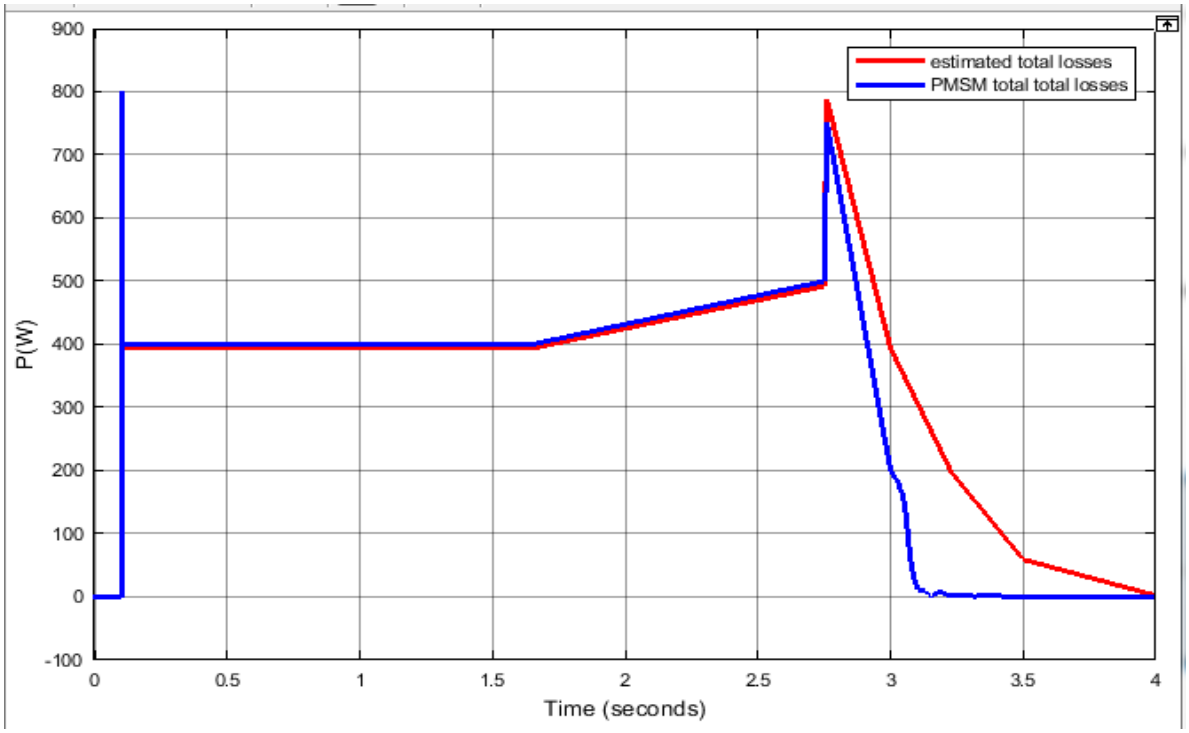

Figure 11: Cure of the estimated total loss by ESO.

To evaluate the performance of ESO tracking the total loss power in the discharge process, the estimated total loss

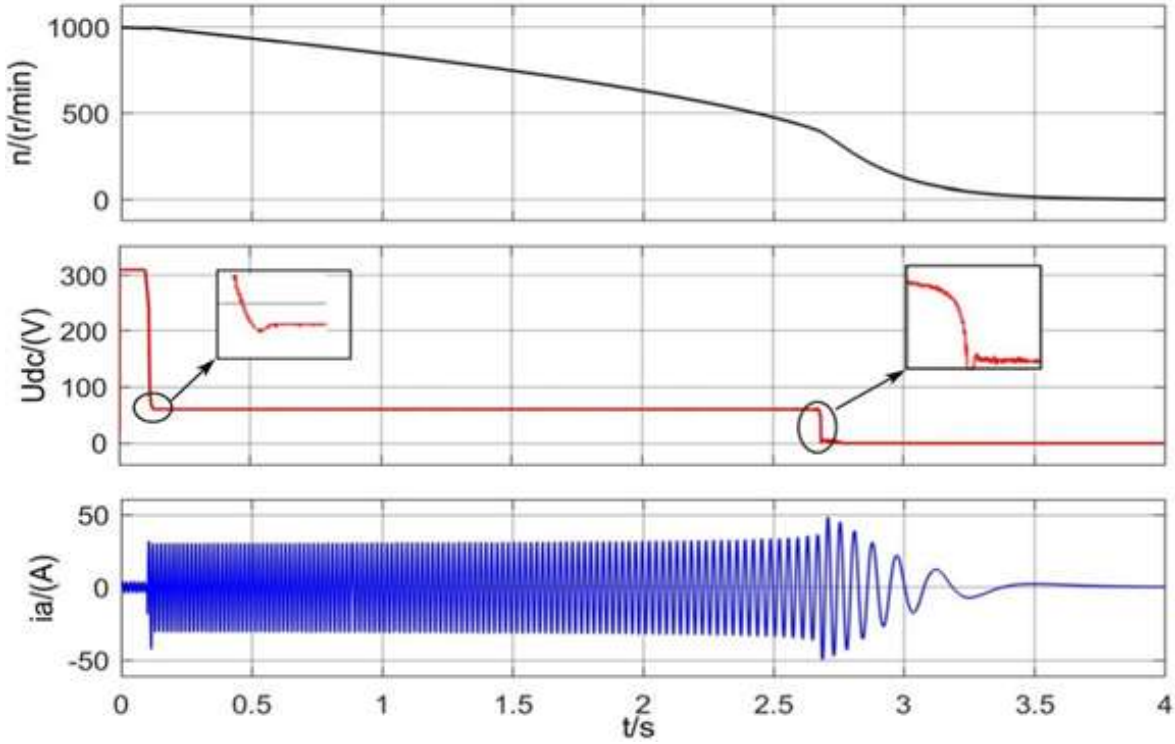

Figure 12: Waveforms of dc-bus capacitor discharge with conventional Пmethod

ISSN: 2278-4632
Vol-13, Issue-07, July 2023

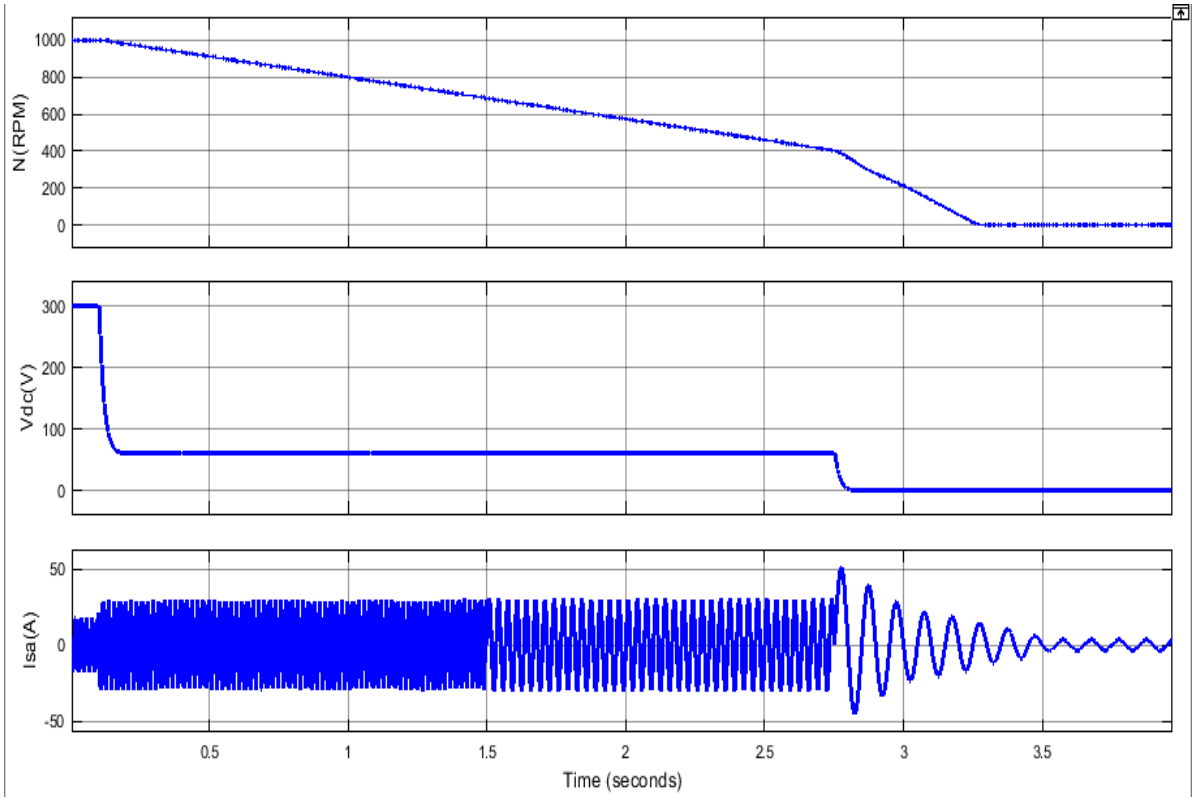

Figure 13: Waveforms of dc-bus capacitor discharge with proposed method.

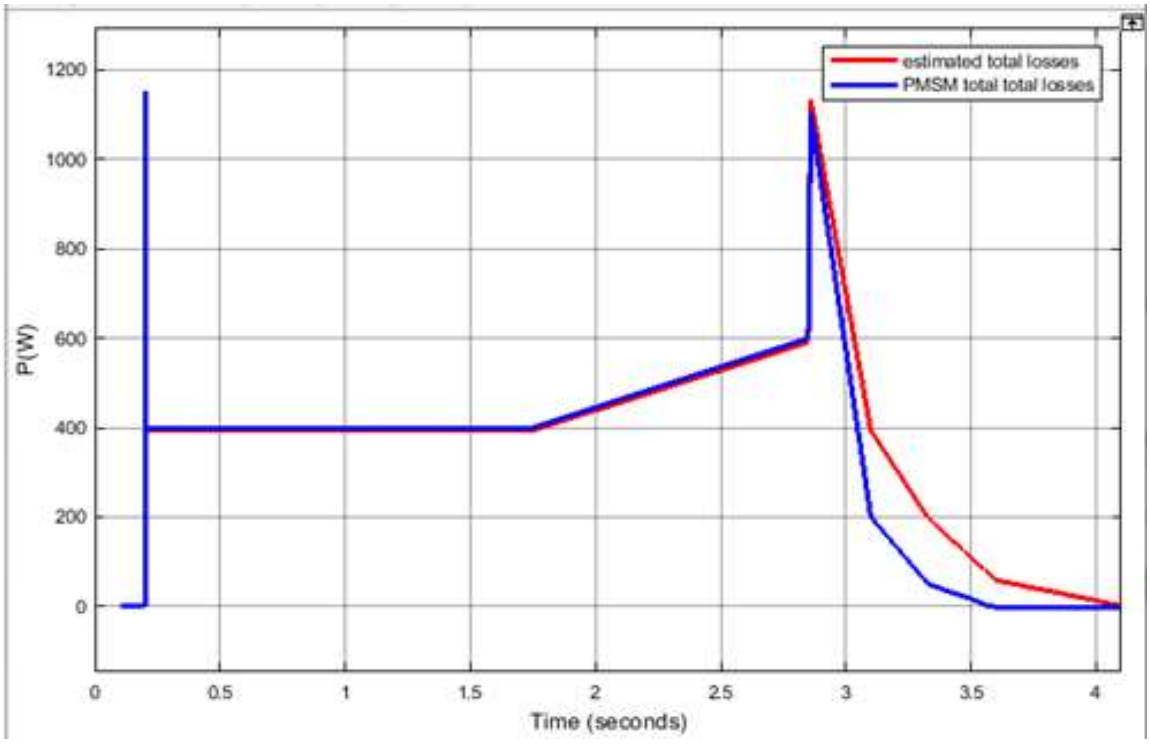

Figure 14: Cure of the estimated total loss by ESO.

ISSN: 2278-4632
Vol-13, Issue-07, July 2023

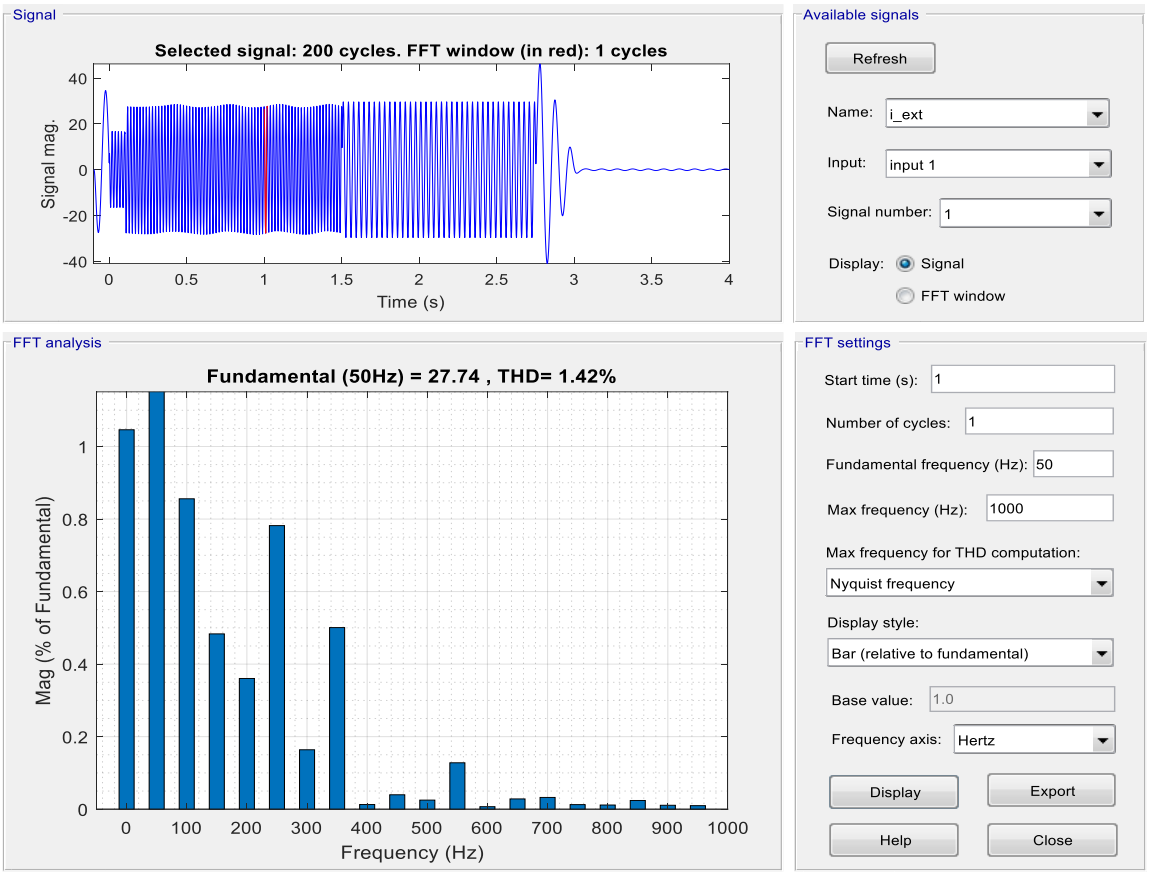

Figure 15: Current THD

by ESO and actual PMSM total loss is compared in Fig.12.

Fig.12 show that the ESO can track the total loss well before*C* point. Since the dc-bus voltage reduce to zero at *C* point, the total loss cannot be observed. In addition, it can be seen that ESO can effectively observe the total loss and compensate it in the control law. These are values used in this.

Table 1: THD Comparison values

Parameter	PI	Fuzzy
Current THD	5.01%	1.42%
Speed settling time	3.25sec	3sec

Symbol	Quantity	Value
Ψ_f	permanent magnetic flux linkage	0.12Wb
L_d	*d*-axis inductance	1.1mH
L_q	*q*-axis inductance	1.1mH
p	number of pole pairs	4
R_S	stator winding resistance	0.307Ω
J	moment of inertia	0.3 kg·m^2
V_{DC}	dc-bus voltage	280V
I_{max}	system safe current	35A
C	dc-bus capacitor	420μF

ISSN: 2278-4632
Vol-13, Issue-07, July 2023

VI.CONCLUSION

A Novel Fuzzy Logic Controller of winding based discharge method can be implemented in this paper. By using fuzzy we are eliminating the voltage & current harmonics that are present in the system. So that power quality of the system can be improved. The performance of fuzzy logic controller is compared with PI under dynamic load condition.

REFERENCES

[1] H. F. Sindi, A. Ul-Haq, M. S. Hassan, A. Iqbal, and M. Jalal, ‘‘Penetration of electric vehicles in Gulf region and its influence on energy and econ- omy,’’ *IEEE Access*, vol. 9, pp. 89412–89431, 2021.

[2] D. Shen, D. Karbowski, and A. Rousseau, ‘‘A minimum principle-based algorithm for energy-efficient eco-driving of electric vehicles in various t

[3] M. Bertoluzzo and G. Buja, ‘‘Development of electric propulsion systems for light electric vehicles,’’ *IEEE Trans. Ind. Informat.*, vol. 7, no. 3, pp. 428–435, Aug. 2011.

[4] D. Fodorean, L. Idoumghar, M. Brévilliers, P. Minciunescu, and C. Irimia, ‘‘Hybrid differential evolution algorithm employed for the optimum design of a high-speed PMSM used for EV propulsion,’’ *IEEE Trans. Ind. Elec- tron.*, vol. 64, no. 12, pp. 9824–9833, Dec. 2017.

[5] C. Gong, Y. Hu, J. Gao, Y. Wang, and L. Yan, ‘‘An improved delay-suppressed sliding-mode observer for sensorless vector-controlled PMSM,’’ *IEEE Trans. Ind. Electron.*, vol. 67, no. 7, pp. 5913–5923, Jul. 2020.

[6] T. Wang, J. Huang, M. Ye, J. Chen, W. Kong, M. Kang, and M. Yu, ‘‘An EMF observer for PMSM sensorless drives adaptive to stator resis- tance and rotor flux linkage,’’ *IEEE J. Emerg. Sel. Topics Power Electron.*, vol. 7, no. 3, pp. 1899–1913, Sep. 2019.

[7] J. Wu, J. Wang, C. Gan, Q. Sun, and W. Kong, ‘‘Efficiency optimization of PMSM drives using field-circuit coupled FEM for EV/HEV applications,’’ *IEEE Access*, vol. 6, pp. 15192–15201, 2018.

[8] H.-S. Kim, S.-K. Sul, H. Yoo, and J. Oh, ‘‘Distortion-minimizing flux observer for IPMSM based on frequency-adaptive observers,’’ *IEEE Trans. Power Electron.*, vol. 35, no. 2, pp. 2077–2087, Feb. 2020.

[9] H. Liu and S. Li, ‘‘Speed control for PMSM servo system using predictive functional control and extended state observer,’’ *IEEE Trans. Ind. Elec- tron.*, vol. 59, no. 2, pp. 1171–1183, Feb. 2012.

[10] C. Gong, Y. Hu, J. Gao, Z. Wu, J. Liu, H. Wen, and Z. Wang, ‘‘Winding- based DC-bus capacitor discharge technique selection principles based on parametric analysis for EV-PMSM drives in post-crash conditions,’’ *IEEE Trans. Power Electron.*, vol. 36, no. 3, pp. 3551–3562, Mar. 2021.

[11] United Nation Economic Commission for Europe Vehicle Regulation, *Unifrom Provisions Concerning the Approval of Vehicles With Regard to the Protection of the Occupants in the Event of a Frontal Collision*, Rev. 2, Annex 11, document no.94 (ECE R94), Aug. 2013.

[12] C. Gong, Y. Hu, W. Li, J. Gao, J. Liu, H. Wen, and J. Yang, ‘‘Hybrid DC-bus capacitor discharge strategy using internal windings and external bleeder for surface-mounted PMSM-based EV powertrains in emergency,’’ *IEEE Trans. Ind. Electron.*, vol. 68, no. 3, pp. 1905–1915, Mar. 2021.

[13] Z. Wu, X. Su, Y. Zhu, and M. Xiao, ‘‘DC link capacitor active discharge by IGBT weak short circuit,’’ *SAE Int. J. Adv. Current Pract. Mobility*, vol. 1, no. 3, pp. 1177–1187, Apr. 2019.

ISSN: 2278-4632
Vol-13, Issue-07, July 2023

[14] T. Goldammer, T. Le, J. Miller, and J. Wai, ‘‘Active high voltage bus bleed down,’’ U.S. Patent 86˙31 894 B2, Jan. 21, 2014.
[15] Z. Ke, J. Zhang, and M. W. Degner, ‘‘DC bus capacitor discharge of permanent-magnet synchronous machine drive systems for hybrid elec- tric vehicles,’’ *IEEE Trans. Ind. Appl.*, vol. 53, no. 2, pp. 1399–1405, Mar. 2017.
[16] C. Gong, Y. Hu, G. Chen, H. Wen, Z. Wang, and K. Ni, ‘‘A DC-bus capacitor discharge strategy for PMSM drive system with large inertia and small system safe current in EVs,’’ *IEEE Trans. Ind. Informat.*, vol. 15, no. 8, pp. 4709–4718, Aug. 2019.
[17] J. Han, ‘‘From PID to active disturbance rejection control,’’ *IEEE Trans. Ind. Electron.*, vol. 56, no. 3, pp. 900–906, Mar. 2009.
[18] D. P. Marcetic and P. R. Matic, ‘‘Nonregenerative braking of permanent magnet synchronous motor,’’ *IEEE Trans. Ind. Electron.*, vol. 67, no. 10, pp. 8186–8196, Oct. 2020.
[19] K. Liu and Z. Q. Zhu, ‘‘Online estimation of the rotor flux linkage and voltage-source inverter nonlinearity in permanent magnet synchronous machine drives,’’ *IEEE Trans. Power Electron.*, vol. 29, no. 1, pp. 418–427, Jan. 2014.
[20] L. Gong, M. Wang, and C. Zhu, ‘‘Immersion and invariance manifold adaptive control of the DC-link voltage in flywheel energy storage system discharge,’’ *IEEE Access*, vol. 8, pp. 144489–144502, 2020.
[21] C. Gong, Y. Hu, C. Gan, G. Chen, and M. Alkahtani, ‘‘Modeling, anal- ysis, and attenuation of uncontrolled generation for IPMSM-based elec- tric vehicles in emergency,’’ *IEEE Trans. Ind. Electron.*, vol. 67, no. 6, pp. 4453–4462, Jun. 2020.
[22] J. Liu, C. Gong, Z. Han, and H. Yu, ‘‘IPMSM model predictive control in flux-weakening operation using an improved algorithm,’’ *IEEE Trans. Ind. Electron.*, vol. 65, no. 12, pp. 9378–9387, Dec. 2018.
[23] Y. Zhang, J. Jin, and L. Huang, ‘‘Model-free predictive current control of PMSM drives based on extended state observer using ultralocal model,’’ *IEEE Trans. Ind. Electron.*, vol. 68, no. 2, pp. 993–1003, Feb. 2021.